Highly Efficient Perovskite Solar Cells with $Ba(OH)_2$ Interface Modification of Mesoporous TiO_2 Electron Transport Layer

M.Thambidurai[1,2], Herlina Arianita Dewi[2], P. C. Harikesh[2], Foo Shini[2,3], K. M. Muhammed Salim[2], Nripan Mathews[2,3], and Cuong Dang[1,2]*

[1]LUMINOUS! Centre of Excellence for Semiconductor Lighting and Displays, School of Electrical & Electronic Engineering, The Photonics Institute (TPI), Nanyang Technological University, 50 Nanyang Avenue, 639798, Singapore.

[2]Energy Research Institute @NTU (ERI@N), Research Techno Plaza, X-Frontier Block, Level 5, 50 Nanyang Drive, 637553, Singapore.

[3]School of Materials Science and Engineering, Nanyang Technological University, 50 Nanyang Avenue, 639798, Singapore.

AUTHOR INFORMATION

Corresponding Author

*Email: hcdang@ntu.edu.sg

KEYWORDS: Perovskite solar cells, barium hydroxide interface, meso-TiO_2, electron transport layer, space charge limited current (SCLC).

ABSTRACT: The outstanding photovoltaic performances together with some advantageous fabrication methods are the driving forces for recent research in perovskite solar devices. Interfacial engineering greatly influences the overall performance of organic-inorganic perovskite solar cell as it alters energy band alignment, carrier recombination, and charge extraction/transport. In this work, $Ba(OH)_2$ was spun between the meso-TiO_2 electron transport and organic-inorganic perovskite absorber layers to engineer the interface and enhance the photovoltaic performance. $Ba(OH)_2$ modification shifted the conduction band of meso-TiO_2 upward such that better alignment with perovskite energy level, reduced carrier recombination, enhanced optical absorption, and electron transportation were observed. These enhancements led to paramount power conversion efficiency (PCE) of 17.53 % for optimum $Ba(OH)_2$ concentration of 5 mg/mL spun on meso-TiO_2, while poorer PCE of 16.08 % for the devices without interfacial treatment. Through this study, we demonstrated the use of interface modification as a straightforward yet powerful approach to enhance performances of conventional perovskite solar cells.

Perovskite-based solar devices have proven to be forceful contenders to existing photovoltaic technologies. Desirable characteristics such as tunable energy band gap, longer carrier lifetime, higher charge mobility, high absorption coefficient, and wide visible light absorption spectrum inspire researchers to believe that perovskites are promising candidates for superior photovoltaic application[1–3]. In a short time, perovskite solar devices have achieved outstanding improvement[4–6] in power conversion efficiency (PCE) from 3.8% to 22%. Typically, a perovskite solar device consists of a TiO_2 electron transport layer (ETL) above the fluorine-doped tin oxide (FTO). The ETL layer is then roughened up by another layer of mesoporous TiO_2 (meso-TiO_2) followed by the perovskite, hole transport, and the metal layer. Upon suitable solar irradiance, excitons are created followed by subsequent charge separation, whereby electrons and holes are injected into the ETL and hole transport layer (HTL) respectively. As such, it is crucial for effective and speedy charge carrier transportation after charge separation or recombination of carriers will take precedence instead. By ensuring proper alignment of energy band levels, efficient charge extraction leading to high device performance can be achieved[7]. On the other hand, incompatible energy levels are believed to deteriorate device performance due to increased carrier recombination and heightened energy barriers at the interfaces.

Modifications to the interface are commonly done via metal doping into the ETL material itself or through interlayer deposition between the ETL/perovskite interface. The use of a befitting interfacial layer is said to provide enhanced device properties due to the presence of interfacial dipole moments and surface passivation[8,9]. Not only will energy levels be altered and better aligned, but edifying interfacial modification could lower the number of trap states, reduce recombination, improve charge extraction/transportation[10,11], thus attaining higher power conversion efficiency. In good agreement, Han et al.[12] reported the use of magnesium oxide (MgO)

coated on meso-TiO_2 to block interfacial recombination at the $MAPbI_3$ and ETL. The addition of CsBr was also reported to enhance the UV stability of the $MAPbI_{3-x}Cl_x$ -based device[13]. In addition, Li et al.[14] demonstrated that CsCl modification allowed better PCE while Shaikh et al.[15] achieved high PCE of 15.81% using simple interfacial modification of meso-TiO_2 ETL with La_2O_3. Moreover, by altering the ETL with Caesium, Dong et al.[16] showed a PCE of 14.2 %. Giordano et al.[17] revealed negligible hysteresis behaviour when conventional meso-TiO_2 was treated with Lithium. Last but not least, Ogomi et al.[18] used Y_2O_3 to passivate the meso-TiO_2 layer resulting in increased PCE from 6.59 % to 7.5 %.

Although uncommon for organic- inorganic perovskite solar cells, $Ba(OH)_2$ is commonly utilized as a superior electron- transporting interlayer in organic semiconductor field effect transistors, polymer light-emitting diodes, and polymer photovoltaic cells[19–21]. By reducing the injection barrier, devices having $Ba(OH)_2$ interlayer displayed higher device performance attributed to better electron injection and reduced recombination. For instance, Zhao et al.[22] utilized $Ba(OH)_2$ as the cathode buffer layer in an inverted polymer solar cell device which led to significant PCE improvement. Borse et al.[23] also showed the addition of $Ba(OH)_2$ to the ZnO ETL in organic solar cells resulting in smaller charge recombination, better charge extraction and hence, superior performance compared to the ZnO counterpart. However, $Ba(OH)_2$ interface modification of mesoporous TiO_2 ETL has been scarcely explored for perovskite solar cells.

In this work, we successfully employed $Ba(OH)_2$ as a new interface modification material between conventional mesoporous TiO_2 ETL and the organic- inorganic perovskite layer. A simple spin coated $Ba(OH)_2$ interface modification on meso-TiO_2 showed an upward shift in conduction band energy, reduced charge recombination, and better electron transport, leading to the improvement in PCE. We optimized the $Ba(OH)_2$ concentration and attained high PCE of 17.53%.

We first characterized the surface morphologies of meso-TiO_2 and meso-TiO_2-$Ba(OH)_2$ using the FESEM to determine possible interfacial modification by $Ba(OH)_2$ on existing meso-TiO_2 surface. The grains in the meso-TiO_2 and meso-TiO_2-$Ba(OH)_2$ samples were all uniform and well-interconnected as shown in supplementary figure S1a,b. The similarity in the FESEM images also suggest that $Ba(OH)_2$ modification has no significant effect on the perovskite morphology deposited on top (supplementary figure S1c, d).

However, $Ba(OH)_2$ modification affect both the chemical and electrical properties of meso-TiO_2. X-ray photoelectron spectroscopy (XPS) was employed to understand the surface composition and chemical state of meso-TiO_2 and meso-TiO_2-$Ba(OH)_2$. Figure 1a indicates the presence of Ti $2p_{3/2,}$ and Ti $2p_{1/2}$ in the meso-TiO_2 sample as represented by the peaks at 458.30 eV and 464.03 eV energies, respectively[24]. On the other hand, slight shifts in Ti $2p_{3/2,}$ and Ti $2p_{1/2}$ binding energies, specifically at 458.16 eV and 463.91 eV, were observed for the meso-TiO_2-$Ba(OH)_2$ sample. This can be explained via the Pauling electronegativity theory. Since Ti atom has a higher electronegativity value of 1.5 compared to 0.89 for Ba atom, which indicates weaker negative charge transfer occurs towards barium in the Ti-O-Ba bond, accounting for the shift in titanium levels to that of lower binding energy [24,25]. Figure 1b shows a slight shift in O 1s binding energy of meso-TiO_2-$Ba(OH)_2$ (529.31 eV) towards lower binding energy as compared to meso-TiO_2 (529.44 eV). Ba $3d_{3/2}$ and $3d_{5/2}$ peaks located at 779.52 eV and 794.78 eV were found in the meso-TiO_2-$Ba(OH)_2$ spectra, while meso-TiO_2 showed the absence of Ba 3d spectra as expected (figure 1c). In meso-TiO_2 only ETL, the atomic percentages of Ti and O were 24.54 % and 75.46 %, respectively while the meso-TiO_2-$Ba(OH)_2$ sample had atomic percentages of Ti, O, and Ba at 14.53 %, 78.18 % and 7.29 %, respectively. The results confirmed the significant amount of Ba in meso-TiO_2-$Ba(OH)_2$ film. This could lead to passivation of oxygen defects via the replacement of

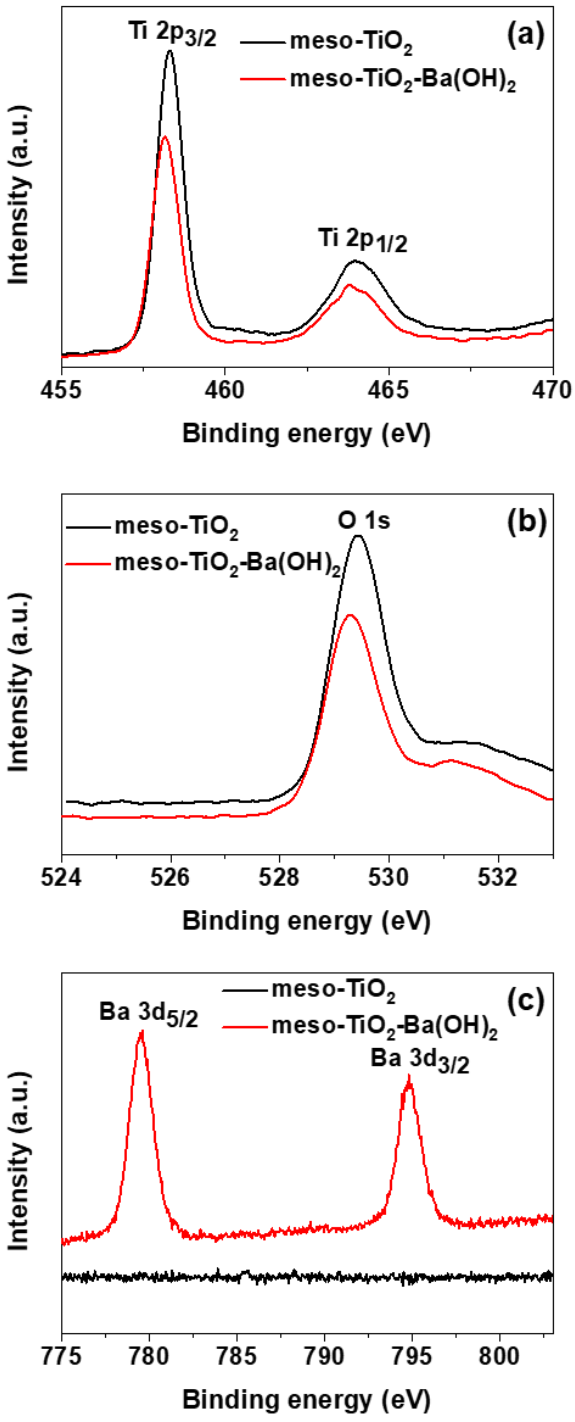

Figure 1. XPS spectra of meso-TiO_2 and meso-TiO_2-$Ba(OH)_2$ films at the peaks of (a) Ti 2p, (b) O 1s, and (c) Ba 3d.

a small Ti portion by Ba as seen for the sample with $Ba(OH)_2$ modification[26]. Figure S2 represents the energy dispersive x-ray diffraction (EDX) spectra of the meso-TiO_2 and the $Ba(OH)_2$-modified meso-TiO_2 samples, revealing the existence of Ba, Ti, and O in meso-TiO_2-$Ba(OH)_2$. The successful formation of a $Ba(OH)_2$ interlayer engineers the meso-TiO_2 chemically.

The energy band alignment among the multiple layers of materials in the solar cell plays an important role in device performance. Figure 2a shows the standard solar device structure wherein the fluorine doped tin oxide (FTO) substrate, TiO_2, perovskite, spiro-OMeTAD, and gold represents the cathode, ETL, active layer, HTL, and anode, respectively. Energy level alignment of samples with and without $Ba(OH)_2$ modifications were determined using the ultraviolet photoelectron spectroscopy (UPS). As recorded, the valence band maximum (E_{VBM}) energies for meso-TiO_2 and meso-TiO_2-$Ba(OH)_2$ ETLs are -7.60 eV and -7.32 eV, respectively. The conduction band minimum (E_{CBM}) levels of the meso-TiO_2 and meso-TiO_2-$Ba(OH)_2$ ETLs could be determined by the valence band maximum and energy band gap (Eg). As shown in figure S3, the plot of $(\alpha h\upsilon)^2$ versus $h\upsilon$ for meso-TiO_2 and meso-TiO_2-$Ba(OH)_2$, the interlayer lowers the optical band gap which was determined by extrapolating the linear portion of the curve to meet the energy axis. In good agreement with the reference values[26], the meso-TiO_2 and meso-TiO_2-$Ba(OH)_2$ ETL have band gaps of 3.59 eV and 3.54 eV, respectively. Conduction band minimum (E_{CBM}) energy levels of the meso-TiO_2 and mesoTiO_2-$Ba(OH)_2$ ETLs are -4.01 eV and -3.82 eV, respectively. Figure 2c represents the energy level diagrams whereby the conduction band of the TiO_2-$Ba(OH)_2$ ETL has shifted slightly upwards compared to that of TiO_2. This decrease in energy offset between the TiO_2-$Ba(OH)_2$ ETL and perovskite layer could enable more effective photogenerated electron transfer.

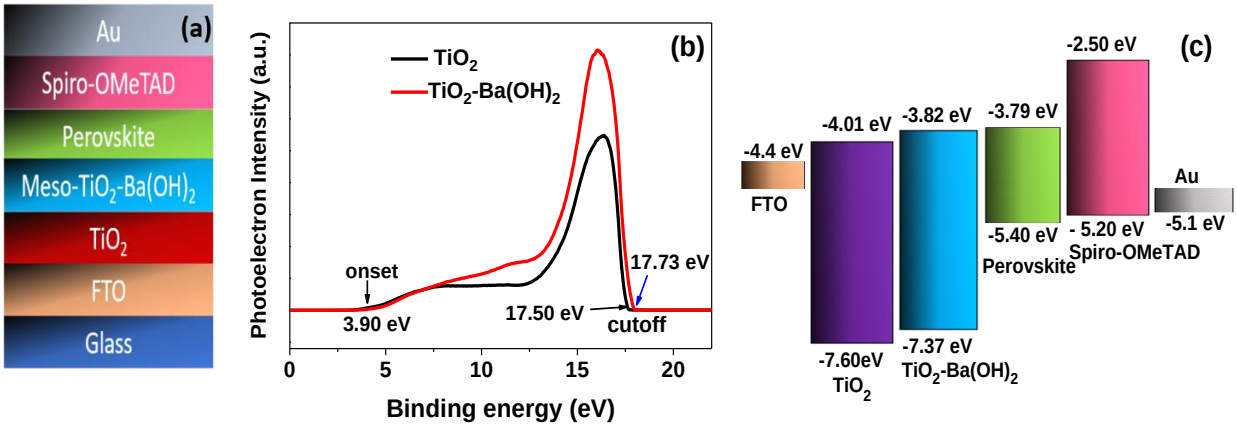

Figure 2. (a) The schematic illustration of the perovskite solar cell device. (b) UPS spectra of meso-TiO_2 and meso-TiO_2-$Ba(OH)_2$ films. (c) Energy level diagram of each layer in the fabricated perovskite solar cells.

To study the effect of $Ba(OH)_2$ interface modification on the performances of perovskite photovoltaics, we constructed and characterized the standard devices based on meso-TiO_2 and meso-TiO_2-$Ba(OH)_2$ ETL. The cross-section of the solar device is depicted in figure 3a by which the FTO substrate is coated with TiO_2, followed by the meso-TiO_2-$Ba(OH)_2$, perovskite, spiro-OMeTAD, and gold layers with estimated thickness of 60, 160, 390, 170, and 80 nm, respectively. We characterized the photovoltaic performance of different $Ba(OH)_2$ concentrations (0, 2, 5, 7, and 10 mg/mL) using the current density–voltage (J–V) curves as shown in figure 3b and S4. Table 1 summarizes the performance of the various devices. Perovskite solar cells with pristine meso-TiO_2 (without $Ba(OH)_2$ modification) exhibited PCE of 16.08 % with an open-circuit voltage (V_{oc}), short-circuit current density (J_{sc}), and fill factor (FF) of 1.04 V, 19.87 mA cm^{-2}, and 77.80 %, respectively. On the other hand, meso-TiO_2-$Ba(OH)_2$ samples showed superior performance for perovskite photovoltaic devices up to 5 mg/mL concentration, after which the performance started to decrease. We achieved the highest performance (PCE) arising out of the high V_{oc}, J_{sc} and

FF when $Ba(OH)_2$ concentration of 5 mg/mL was employed. More specifically, the best device demonstrated the highest PCE of 17.53% with V_{oc}, J_{sc}, FF of 1.09 V, 20.81 mA cm^{-2}, and 77.51 %, respectively. However, further increase in $Ba(OH)_2$ concentration resulted in the decrease in PCE as seen at 17.03 % and 16.75 % for devices for 7 and 10 mg/mL devices, respectively.

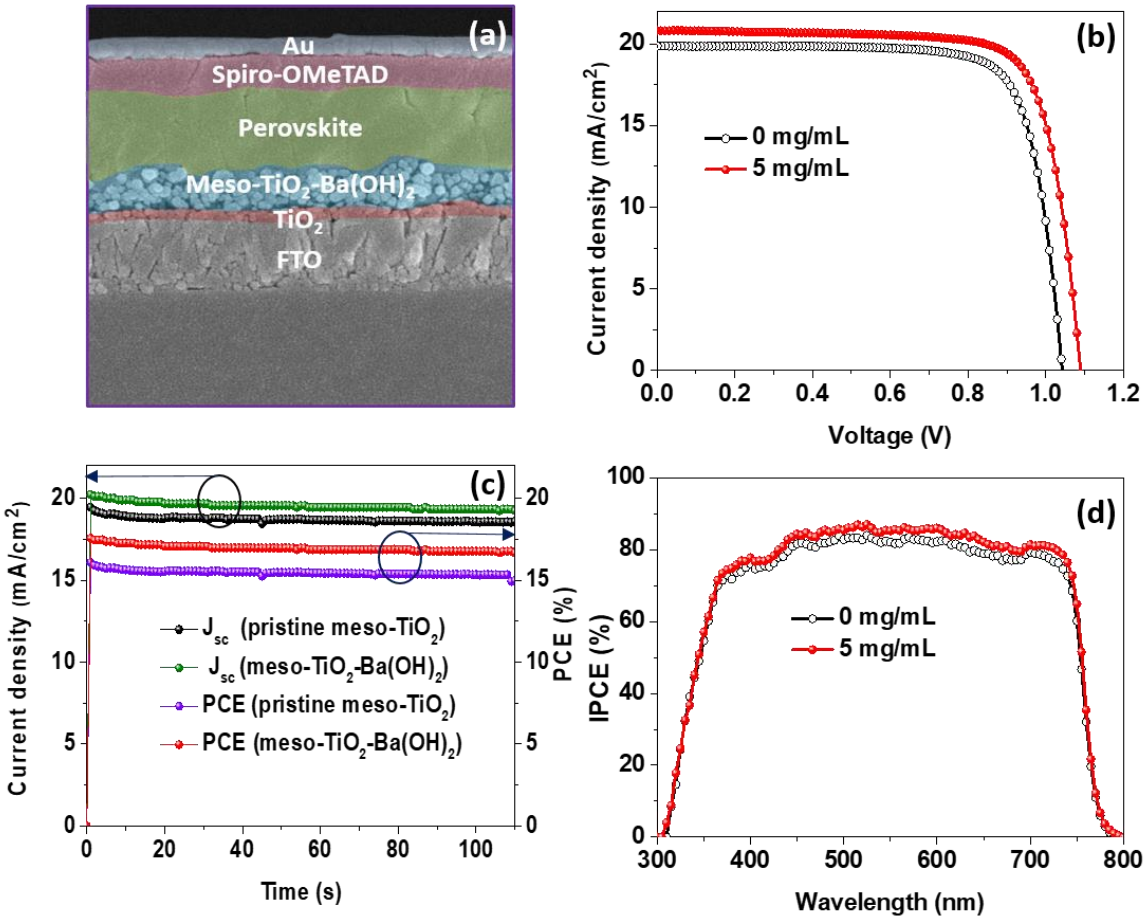

Figure 3. (a) Cross-sectional SEM image of the device with $Ba(OH)_2$ interface modification. (b) Current density-voltage (J-V) characteristics of the meso-TiO_2 and meso-TiO_2-$Ba(OH)_2$ ETL based perovskite solar cells under reverse scanning (RS). (c) The steady state efficiency of the pristine meso-TiO_2 and 5 mg/mL $Ba(OH)_2$ modified meso-TiO_2 based perovskite devices measured at maximum power output. (d) IPCE spectra of perovskite solar cells with meso-TiO_2 and meso-TiO_2-$Ba(OH)_2$ ETLs.

As seen in figure 3c, the steady state efficiencies of the pristine meso-TiO_2 and meso-TiO_2-$Ba(OH)_2$ based devices were also conducted. The pristine meso-TiO_2 based device showed a stable J_{sc} of 18.71 mA/cm^2 and PCE of 15.10 % at voltage bias of 0.82 V. In comparison, the meso-TiO_2-$Ba(OH)_2$ based device exhibited a stable J_{sc} of 19.54 mA/cm^2 and a stable PCE of 16.95 % at voltage bias of 0.87 V. The higher steady state output of meso-TiO_2-$Ba(OH)_2$ based device observed is probably caused by the faster charge transfer and suppressed charge recombination due to the improved contact properties between perovskite and meso-TiO_2-$Ba(OH)_2$ ETL.

Table 1: Photovoltaic parameters of the meso-TiO_2 and meso-TiO_2-$Ba(OH)_2$ based perovskite device measured under a standard AM 1.5G illumination of 100 mW cm^{-2}.

$Ba(OH)_2$ modification	Scan direction	Voc [V]	Jsc [mA cm-2]	FF [%]	PCE [%]
0 mg/mL	reverse	1.04	19.87	77.80	16.08
	forward	1.03	19.28	68.78	13.67
2 mg/mL	reverse	1.06	20.07	77.95	16.53
	forward	1.02	20.15	69.94	14.44
5 mg/mL	reverse	1.09	20.81	77.51	17.53
	forward	1.06	20.79	69.15	15.18
7 mg/mL	reverse	1.08	20.64	76.71	17.03
	forward	1.04	20.65	66.19	14.20
10 mg/mL	reverse	1.08	20.31	76.47	16.75
	forward	1.04	20.29	66.64	14.13

Optimization was done thoroughly together with device reproducibility which was verified using statistical distribution of the photovoltaic parameters. As seen in figure S5, the statistics analysis confirmed that almost all tested devices with meso-TiO_2-$Ba(OH)_2$ had higher PCE when compared to pristine meso-TiO_2 device. The average PCE of meso-TiO_2 and meso-TiO_2-$Ba(OH)_2$ based devices are 15.23 % and 17.04 %, respectively. In addition, the stability of all the perovskite devices in the absence of encapsulation was conducted. As seen in figure S6, the meso-TiO_2 and meso-TiO_2-$Ba(OH)_2$ based devices retained 90 % and 96 % of their initial PCE value even after storage under ambient conditions for 25 days. The meso-TiO_2 device which retained 90% of its initial PCE attained V_{oc}, J_{sc}, FF, and PCE are 1.04 V, 19.62 mA/cm^2, 71.93, and 14.77 %, respectively. On the other hand, the meso-TiO_2-$Ba(OH)_2$ device that retained 96% of its initial PCE had V_{oc}, J_{sc}, FF, and PCE of 1.08 V, 20.44 mA/cm^2, 75.55, and 16.79 %, respectively. We postulate that one possible factor for the better stability could be due to the reduced amount of traps in the TiO_2 layer when $Ba(OH)_2$ is added. As such, improved charge transfer between TiO_2 and perovskite is observed due to the suppression of charge accumulation and recombination.

The IPCE spectra (figure 3d) can provide detailed spectrum response of the photovoltaic device. Throughout the entire wavelength range, superior charge injection and transportation in the $Ba(OH)_2$ interlayer device was reflected via its higher IPCE compared to that in the pristine meso-TiO_2 device. From figure 3d, the J_{sc} values for $Ba(OH)_2$ interlayer perovskite devices are calculated to be 19.42, 19.59, 20.17, 19.86, and 19.77 mA cm^{-2} corresponding to the 0, 2, 5, 7, and 10 mg/mL $Ba(OH)_2$ concentrations, which are in good agreement with Table 1 measured under full sun illumination.

The trap densities of TiO_2 and TiO_2-$Ba(OH)_2$ films with different $Ba(OH)_2$ concentrations (2, 5, 7 and 10 mg/mL) were measured by the space charge limited current (SCLC) method as shown in

figure S7 and Table S1. The relationship between trap filled limit voltage (V_{TFL}) and trap density (N_t) follows the equation of $V_{TFL} = eN_t d^2/2\varepsilon\varepsilon_0$, where e is the elementary charge (1.6×10^{-19} C), d (~60 nm) is the film thickness, ε_0 is the vacuum permittivity (8.85×10^{-12} Fm^{-1}), ε is the relative dielectric constant of anatase TiO_2 (~55 Fm^{-1}), and N_t is the trap density[30]. The trap filled limit voltage (V_{TFL}) of TiO_2 based device (1.17 V) is higher than that of 5 mg/mL of $Ba(OH)_2$ based device (0.58 V). By using the equation as mentioned above, the calculated trap density of TiO_2 and of 5 mg/mL of $Ba(OH)_2$ modified TiO_2 are 1.97×10^{18} cm^{-3} and 0.98×10^{18} cm^{-3}, respectively. This indicates that $Ba(OH)_2$ modification reduces the number of defects states. However, as seen from the SCLC results, further increase in $Ba(OH)_2$ concentrations creates more traps.

Transmittance spectra of meso-TiO_2 and meso-TiO_2-$Ba(OH)_2$ ETLs are shown in figure 4a. The meso-TiO_2 and meso-TiO_2-$Ba(OH)_2$ displayed high transmissivity in the UV-VIS range while a little reduction in the range from 370 nm to 520 nm for meso-TiO_2-$Ba(OH)_2$ compared to pristine meso-TiO_2. The optical absorption spectra of glass/perovskite, meso-TiO_2/perovskite, meso-TiO_2-$Ba(OH)_2$/perovskite films are shown in figure 4b. A plausible cause for the increased J_{sc} observed in the meso-TiO_2-$Ba(OH)_2$/perovskite film is the enhanced light absorption in the wavelength range of 500-750 nm. Figure 4c shows the PL spectra of glass/perovskite, meso-TiO_2/perovskite, meso-TiO_2-$Ba(OH)_2$/perovskite films. The glass/perovskite film showed the highest PL intensity, indicating significant carrier recombination. However, meso-TiO_2-$Ba(OH)_2$/perovskite film displayed lower intensity compared to the sample without $Ba(OH)_2$. This demonstrates faster charge extraction from perovskite to meso-TiO_2 when $Ba(OH)_2$ interlayer is introduced. In the presence of $Ba(OH)_2$, it is believed that successful passivation of oxygen defects found within the ETL/perovskite interface has occurred, resulting in recombination reduction, improved charge extraction, and hence enhanced J_{sc}[26].

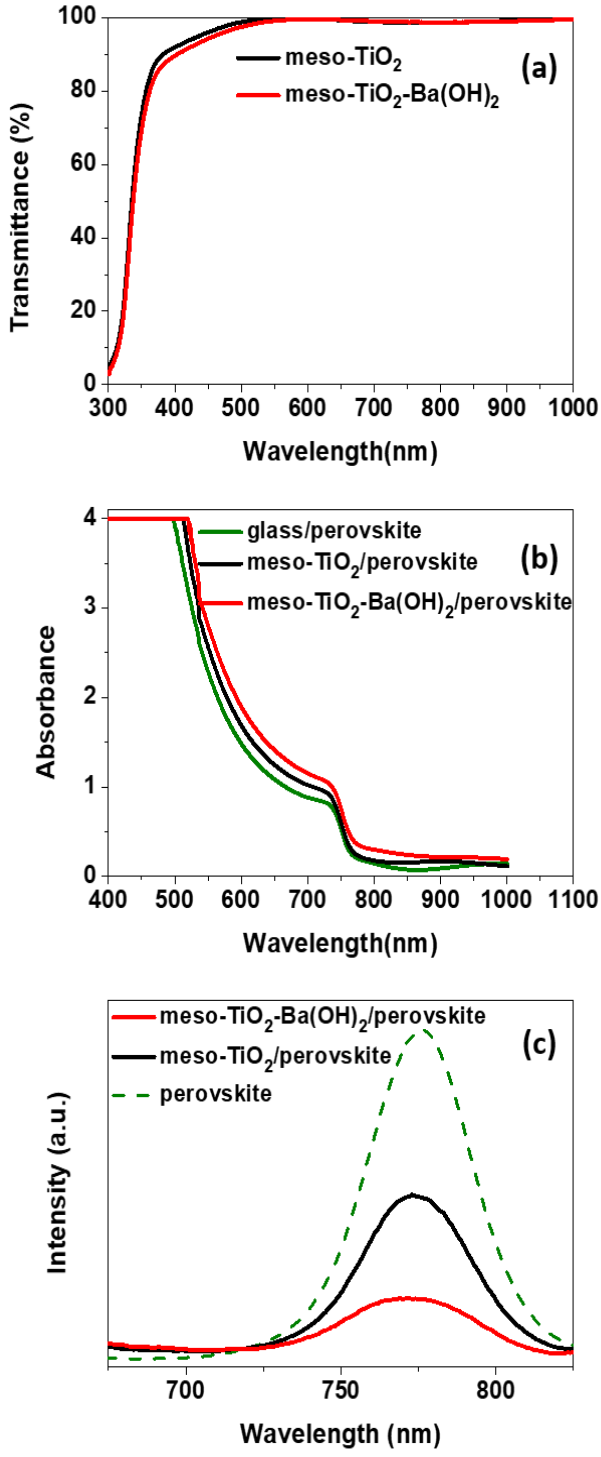

Figure 4. (a) Optical transmittance spectra of meso-TiO_2 and meso-TiO_2-$Ba(OH)_2$ ETLs. (b) Optical absorption spectra and (c) PL spectra of perovskite, meso-TiO_2/perovskite and meso-TiO_2-$Ba(OH)_2$/ perovskite films.

Electrochemical impedance spectroscopy (EIS) was utilized to investigate the charge transfer and recombination dynamics of the samples[27]. Figure 5 represents the Nyquist plots for meso-TiO_2 and meso-TiO_2-$Ba(OH)_2$ devices under dark condition with a forward bias of 800 mV. According to the Nyquist plot, there are two arcs observed; the first arc at higher frequency is generally associated with the intrinsic dielectric relaxation of perovskite layer and the contact transport resistance, while the other arc corresponds to the recombination resistance and chemical capacitance[28]. As seen in figure S8, the equivalent circuit[29] is made up of a series resistance (R_s), two capacitive (C_1 and C_2) and two resistive components (R_{rec} and R_1). The results are summarized in Table S2 showing that larger recombination resistance (R_{rec}) and smaller series resistance (R_{series}) was observed for 5 mg/mL of $Ba(OH)_2$ modified meso-TiO_2 device when compared to pristine meso-TiO_2 device. This evidence of enhanced charge transport and reduced recombination observed in the meso-TiO_2-$Ba(OH)_2$ device further reinforce the observed improvement in V_{oc} and J_{sc}. However, when too high an amount of $Ba(OH)_2$ is added, a significant decrease in R_{rec} is observed, resulting in higher recombination. This can be seen in the 10mg/mL $Ba(OH)_2$ modified meso-TiO_2 device.

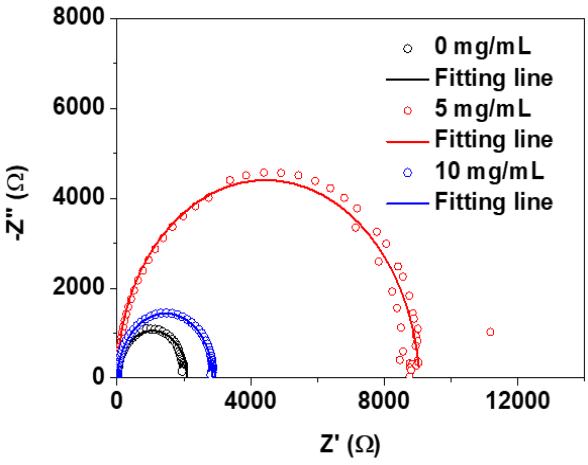

Figure 5. Nyquist plot for perovskite devices with meso-TiO_2 and meso-TiO_2-$Ba(OH)_2$ ETLs.

In summary, effective use of $Ba(OH)_2$ on ETL was demonstrated in perovskite solar devices. $Ba(OH)_2$ solution was spun over the meso-TiO_2 layer, whereby controlled samples (without $Ba(OH)_2$ modification) only attained PCE of 16.08% while the optimum $Ba(OH)_2$ concentration of 5 mg/mL exhibited paramount performance with PCE, V_{oc}, J_{sc}, and FF of 17.53%, 1.09 V, 20.81 mA cm^{-2}, and 77.51 %, respectively. We identified the origins of such high performance in multiple device experiments and material characterizations. The upward shift in conduction band energy level to that closer to the perovskite energy level lifts the overall V_{oc}. On the other hand, enhanced optical absorption and reduced carrier recombination in the meso-TiO_2-$Ba(OH)_2$/perovskite films increase the J_{sc}. The larger recombination resistance (R_{rec}) and smaller series resistance (R_{series}) revealed in the EIS results of $Ba(OH)_2$ modified perovskite photovoltaic devices further confirmed the better electron transportation and collection, leading to the as-observed improvement in V_{oc} and J_{sc}. Through this study, it is evident that the employment of simple interface modification using $Ba(OH)_2$ could significantly enhance perovskite photovoltaic devices.

ASSOCIATED CONTENT

Supporting Information

Experimental details, characterization method, FESEM images, EDX, band gap values, current density (J-V), space charge limited current (SCLC) and equivalent circuit.

AUTHOR INFORMATION

*Email: hcdang@ntu.edu.sg

Notes

The authors declare no competing financial interest.

ACKNOWLEDGMENT

The research is supported by AcRF Tier1 grant (RG 178/17) from Singapore Ministry of Education. We would like to thank Prof. Subodh Mhaisalkar, Executive Director of Energy Research Institute @ NTU (ERI@N) for supporting this work.

REFERENCES

(1) Xing, G.; Mathews, N.; Sun, S.; Lim, S. S.; Lam, Y. M.; Gratzel, M.; Mhaisalkar, S.; Sum, T. C. Long-Range Balanced Electron and Hole-Transport Lengths in Organic-Inorganic $CH_3NH_3PbI_3$. *Science* **2013**, *342*, 344–347.

(2) Correa-Baena, J.-P.; Abate, A.; Saliba, M.; Tress, W.; Jesper Jacobsson, T.; Grätzel, M.; Hagfeldt, A. The Rapid Evolution of Highly Efficient Perovskite Solar Cells. *Energy Environ. Sci.* **2017**, *10*, 710–727.

(3) Salim, K. M. M.; Koh, T. M.; Bahulayan, D.; Harikesh, P. C.; Jamaludin, N. F.; Febriansyah, B.; Bruno, A.; Mhaisalkar, S.; Mathews, N. Extended Absorption Window and Improved Stability of Cesium-Based Triple-Cation Perovskite Solar Cells Passivated with Perfluorinated Organics. *ACS Energy Lett.* **2018**, *3*, 1068–1076.

(4) Akihiro Kojima; Teshima, K.; Shirai, Y.; Miyasaka, T. Organometal Halide Perovskites as Visible- Light Sensitizers for Photovoltaic Cells. *J Am Chem Soc* **2009**, *131*, 6050–6051.

(5) Shin, S. S.; Yeom, E. J.; Yang, W. S.; Hur, S.; Kim, M. G.; Im, J.; Seo, J.; Noh, J. H.; Seok, S. Il. Colloidally Prepared La-Doped $BaSnO_3$ Electrodes for Efficient, Photostable Perovskite Solar Cells. *Science* **2017**, *356*, 167–171.

(6) Saliba, M.; Matsui, T.; Seo, J.-Y.; Domanski, K.; Correa-Baena, J.-P.; Nazeeruddin, M. K.;

Zakeeruddin, S. M.; Tress, W.; Abate, A.; Hagfeldt, A. Cesium-Containing Triple Cation Perovskite Solar Cells: Improved Stability, Reproducibility and High Efficiency. *Energy Environ. Sci.* **2016**, *9*, 1989–1997.

(7) Correa Baena, J. P.; Steier, L.; Tress, W.; Saliba, M.; Neutzner, S.; Matsui, T.; Giordano, F.; Jacobsson, T. J.; Srimath Kandada, A. R.; Zakeeruddin, S. M.; et al. Highly Efficient Planar Perovskite Solar Cells through Band Alignment Engineering. *Energy Environ. Sci.* **2015**, *8*, 2928–2934.

(8) Page, Z. A.; Duzhko, V. V.; Emrick, T. Conjugated Thiophene-Containing Polymer Zwitterions: Direct Synthesis and Thin Film Electronic Properties. *Macromolecules* **2013**, *46*, 344–351.

(9) Li, H.; Tao, L.; Huang, F.; Sun, Q.; Zhao, X.; Han, J.; Shen, Y.; Wang, M. Enhancing Efficiency of Perovskite Solar Cells via Surface Passivation with Graphene Oxide Interlayer. *ACS Appl. Mater. Interfaces* **2017**, 9, 38967-38976.

(10) Lim, K.-G.; Ahn, S.; Lee, T.-W. Energy Level Alignment of Dipolar Interface Layer in Organic and Hybrid Perovskite Solar Cells. *J. Mater. Chem. C* **2018**, *6*, 2915–2924.

(11) Guo, Q.; Xu, Y.; Xiao, B.; Zhang, B.; Zhou, E.; Wang, F.; Bai, Y.; Hayat, T.; Alsaedi, A.; Tan, Z. Effect of Energy Alignment, Electron Mobility, and Film Morphology of Perylene Diimide Based Polymers as Electron Transport Layer on the Performance of Perovskite Solar Cells. *ACS Appl. Mater. Interfaces* **2017**, *9*, 10983–10991.

(12) Han, G. S.; Chung, H. S.; Kim, B. J.; Kim, D. H.; Lee, J. W.; Swain, B. S.; Mahmood, K.; Yoo, J. S.; Park, N.-G.; Lee, J. H.; et al. Retarding Charge Recombination in Perovskite

Solar Cells Using Ultrathin MgO-Coated TiO_2 Nanoparticulate Films. *J. Mater. Chem. A* **2015**, *3*, 9160–9164.

(13) Li, W.; Zhang, W.; Van Reenen, S.; Sutton, R. J.; Fan, J.; Haghighirad, A. A.; Johnston, M. B.; Wang, L.; Snaith, H. J. Enhanced UV-Light Stability of Planar Heterojunction Perovskite Solar Cells with Caesium Bromide Interface Modification. *Energy Environ. Sci.* **2016**, *9*, 490–498.

(14) Li, W.; Li, J.; Niu, G.; Wang, L. Effect of Cesium Chloride Modification on the Film Morphology and UV-Induced Stability of Planar Perovskite Solar Cells. *J. Mater. Chem. A* **2016**, *4*, 11688–11695.

(15) Shaikh, S. F.; Kwon, H.-C.; Yang, W.; Hwang, H.; Lee, H.; Lee, E.; Ma, S.; Moon, J. La_2O_3 Interface Modification of Mesoporous TiO_2 Nanostructures Enabling Highly Efficient Perovskite Solar Cells. *J. Mater. Chem. A* **2016**, *4*, 15478–15485.

(16) Dong, H.; Guo, X.; Li, W.; Wang, L. Cesium Carbonate as a Surface Modification Material for Organic–inorganic Hybrid Perovskite Solar Cells with Enhanced Performance. *RSC Adv.* **2014**, *4*, 60131–60134.

(17) Giordano, F.; Abate, A.; Correa Baena, J. P.; Saliba, M.; Matsui, T.; Im, S. H.; Zakeeruddin, S. M.; Nazeeruddin, M. K.; Hagfeldt, A.; Graetzel, M. Enhanced Electronic Properties in Mesoporous TiO_2 via Lithium Doping for High-Efficiency Perovskite Solar Cells. *Nat. Commun.* **2016**, *7*, 10379.

(18) Ogomi, Y.; Kukihara, K.; Qing, S.; Toyoda, T.; Yoshino, K.; Pandey, S.; Momose, H.; Hayase, S. Control of Charge Dynamics through a Charge-Separation Interface for All-

Solid Perovskite-Sensitized Solar Cells. *ChemPhysChem* **2014**, *15*, 1062–1069.

(19) Kim, N. K.; Khim, D.; Xu, Y.; Lee, S. H.; Kang, M.; Kim, J.; Facchetti, A.; Noh, Y. Y.; Kim, D. Y. Solution-Processed Barium Salts as Charge Injection Layers for High Performance N-Channel Organic Field-Effect Transistors. *ACS Appl. Mater. Interfaces* **2014**, *6*, 9614–9621.

(20) Lu, L. P.; Kabra, D.; Friend, R. H. Barium Hydroxide as an Interlayer between Zinc Oxide and a Luminescent Conjugated Polymer for Light-Emitting Diodes. *Adv. Funct. Mater.* **2012**, *22*, 4165–4171.

(21) Zhao, W.; Ye, L.; Zhang, S.; Yao, H.; Sun, M.; Hou, J. An Easily Accessible Cathode Buffer Layer for Achieving Multiple High Performance Polymer Photovoltaic Cells. *J. Phys. Chem. C* **2015**, *119*, 27322–27329.

(22) Zhang, H.; Stubhan, T.; Li, N.; Turbiez, M.; Matt, G. J.; Ameri, T.; Brabec, C. J. A Solution-Processed Barium Hydroxide Modified Aluminum Doped Zinc Oxide Layer for Highly Efficient Inverted Organic Solar Cells. *J. Mater. Chem. A* **2014**, *2*, 18917–18923.

(23) Borse, K.; Sharma, R.; Gupta, D.; Yella, A. Interface Engineering through Electron Transport Layer Modification for High Efficiency Organic Solar Cells. *RSC Adv.* **2018**, *8*, 5984–5991.

(24) Li, X.; Yang, J.; Jiang, Q.; Chu, W.; Zhang, D.; Zhou, Z.; Xin, J. Synergistic Effect to High-Performance Perovskite Solar Cells with Reduced Hysteresis and Improved Stability by the Introduction of Na-Treated TiO_2 and Spraying-Deposited CuI as Transport Layers. *ACS Appl. Mater. Interfaces* **2017**, *9*, 41354–41362.

(25) Reddy, B. M.; Chowdhury, B.; Smirniotis, P. G. An XPS Study of La_2O_3 and In_2O_3 Influence on the Physicochemical Properties of MoO_3/TiO_2 Catalysts. *Appl. Catal. A Gen.* **2001**, *219*, 53–60.

(26) Sidhik, S.; Cerdan Pasarán, A.; Esparza, D.; López Luke, T.; Carriles, R.; De la Rosa, E. Improving the Optoelectronic Properties of Mesoporous TiO_2 by Cobalt Doping for High-Performance Hysteresis-Free Perovskite Solar Cells. *ACS Appl. Mater. Interfaces* **2018**, 10, 3571-3580.

(27) Ke, W.; Zhao, D.; Cimaroli, A. J.; Grice, C. R.; Qin, P.; Liu, Q.; Xiong, L.; Yan, Y.; Fang, G. Effects of Annealing Temperature of Tin Oxide Electron Selective Layers on the Performance of Perovskite Solar Cells. *J. Mater. Chem. A* **2015**, *3*, 24163–24168.

(28) Cai, Q.; Zhang, Y.; Liang, C.; Li, P.; Gu, H.; Liu, X.; Wang, J.; Shentu, Z.; Fan, J.; Shao, G. Enhancing Efficiency of Planar Structure Perovskite Solar Cells Using Sn-Doped TiO_2 as Electron Transport Layer at Low Temperature. *Electrochim. Acta* **2018**, *261*, 227–235.

(29) Zarazua, I.; Han, G.; Boix, P. P.; Mhaisalkar, S.; Fabregat-Santiago, F.; Mora-Seró, I.; Bisquert, J.; Garcia-Belmonte, G. Surface Recombination and Collection Efficiency in Perovskite Solar Cells from Impedance Analysis. *J. Phys. Chem. Lett.* **2016**, *7*, 5105–5113.

(30) Lv, Y.; Cai, B.; Ma, Q.; Wang, Z.; Liu, J.; Zhang, W.-H. Highly Crystalline Nb-Doped TiO_2 Nanospindles as Superior Electron Transporting Materials for High-Performance Planar Structured Perovskite Solar Cells. *RSC Adv.* **2018**, *8*, 20982–20989.

TOC GRAPHICS

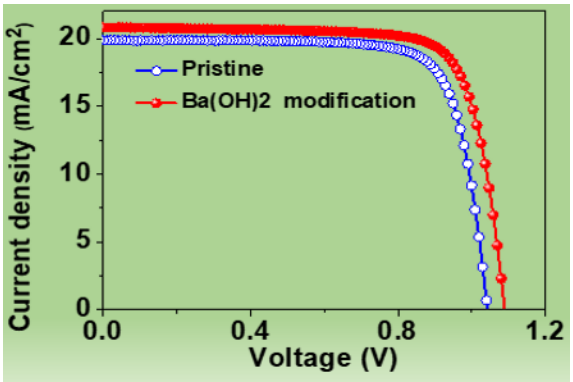

Supporting information

Highly Efficient Perovskite Solar Cells with $Ba(OH)_2$ Interface Modification of Mesoporous TiO_2 Electron Transport Layer

M.Thambidurai[1,2], Herlina Arianita Dewi[2], P. C. Harikesh[2], Foo Shini[2,3], K.M. Muhammed Salim[2], Nripan Mathews[2,3], and Cuong Dang[1,2]*

[1]LUMINOUS! Centre of Excellence for Semiconductor Lighting and Displays, School of Electrical & Electronic Engineering, The Photonics Institute (TPI), Nanyang Technological University, 50 Nanyang Avenue, 639798, Singapore.

[2]Energy Research Institute @NTU (ERI@N), Research Techno Plaza, X-Frontier Block, Level 5, 50 Nanyang Drive, 637553, Singapore.

[3]School of Materials Science and Engineering, Nanyang Technological University, 50 Nanyang Avenue, 639798, Singapore.

AUTHOR INFORMATION

Corresponding Author

*Email: hcdang@ntu.edu.sg

Experiments

Purchased fluorine-doped tin oxide (FTO, Nippon sheet glass Co., Ltd., Japan) glass substrates were patterned by etching with Zn powder and HCl. The patterned FTO glass substrates were cleaned using detergent, deionized water, acetone, ethanol, isopropyl alcohol and dried under nitrogen, followed by oxygen plasma treatment for 10 min. A compact TiO_2 layer was spun onto the surface of the substrate using a solution consisting of titanium (IV) butoxide, 2-methoxyethanol and acetylacetone. For 30 s, the high surface area meso-TiO_2 was spin coated at 5000 rpm using ethanol diluted TiO_2 paste (30NR-T) in a weight ratio of 1:5.5, followed by the deposition of dissolved $Ba(OH)_2$ in 2-methoxyethanol (0, 2, 5, 7 and 10 mg/mL concentration) at 3000 rpm for 30 s. The as-prepared sample was then annealed for 15 min at 150 ºC. Afterward, the perovskite solution was prepared using PbI_2 (1.1 M), FAI (1.0 M), $PbBr_2$ (0.22 M), and MABr (0.2 M) dissolved in 1 mL of anhydrous DMF: DMSO (4:1 volume ratio). In addition, 42 µL of CsI (1.5 M) stock solution was added to the perovskite solution prior to two separate spin coating steps at 2000 rpm for 10 s and 6000 rpm for 30 s. At the last 15 s, 100 µL of chlorobenzene was drop casted onto the surface of the sample and annealed at 100 ºC for 1 h. Next, a thin layer of Spiro-OMeTAD was spun at 5000 rpm for 30 s using a mixture consisting of 70 mg Spiro-OMeTAD, 28 µL 4-tert-butylpyridine, 16.94 µL bis(trifluoromethylsulfonyl)amine lithium salt (520 mg/mL in acetonitrile), and 35 µL FK209 Co(III) TFSI Salt (18.8 mg/50 µL in acetonitrile) dissolved in 1 mL of chlorobenzene. Finally, the thermal evaporator was employed to deposit 80 nm of gold as the metal contact.

Characterization: Surface morphological and chemical characteristics were analysed under field emission scanning electron microscope (FESEM; JEJOL JSM-7600F) and X-ray photoelectron spectroscopy (XPS), respectively. Ultraviolet photoelectron spectroscopy (UPS) measurement was

conducted with AXIS Ultra DLD (KRATOS Inc.). Current density against voltage (J-V) plots were recorded under one-sun AM 1.5G (100 mW/cm^2) using the Keithley 2612A source meter. The light intensity was calibrated against the traditional silicon solar cell. UV-VIS spectrophotometer (Shimadzu, UV-1800) and spectrofluorophotometer (Shimadzu, RF-5301PC) were employed to record the absorption, transmittance spectra and photoluminescence (PL) spectra, respectively. Incident photon-to-current conversion (IPCE) was calculated using PVE300 (Bentham). Impedance spectroscopy (Autolab PGSTAT302N) was conducted under dark condition by applying a perturbation of frequencies varying from 10 Hz to 1 MHz at a DC voltage of 700 mV.

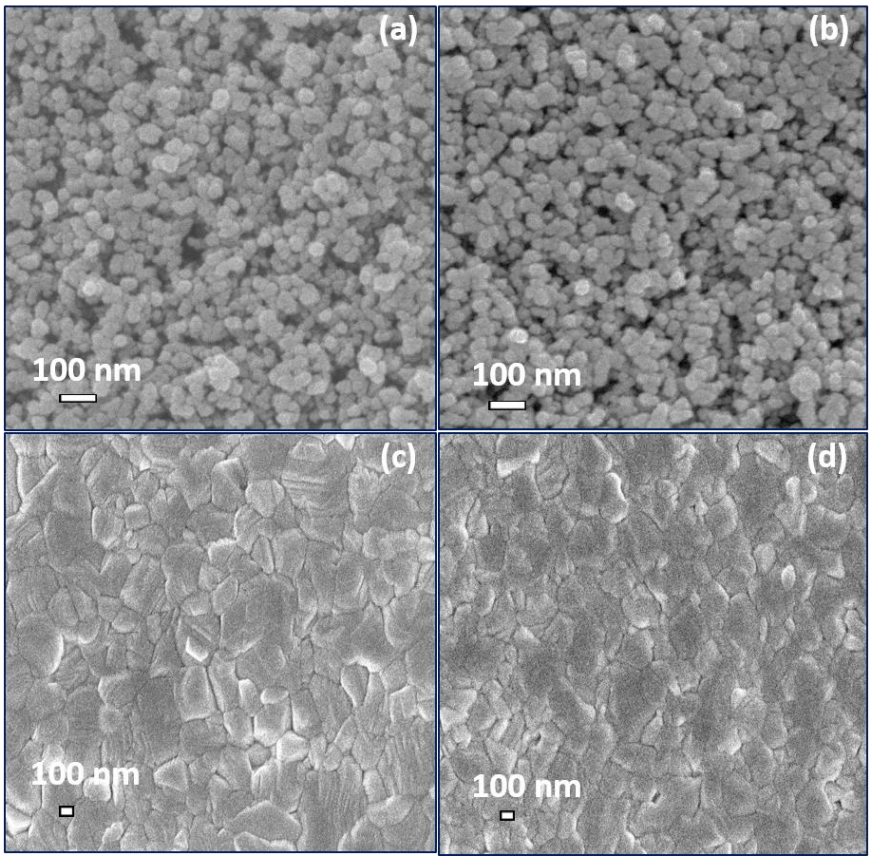

Figure S1. FESEM images of (a) meso-TiO_2 and (b) meso-TiO_2-$Ba(OH)_2$. FESEM images of the perovskite films deposited on a (c) meso-TiO_2 and (d) meso-TiO_2-$Ba(OH)_2$.

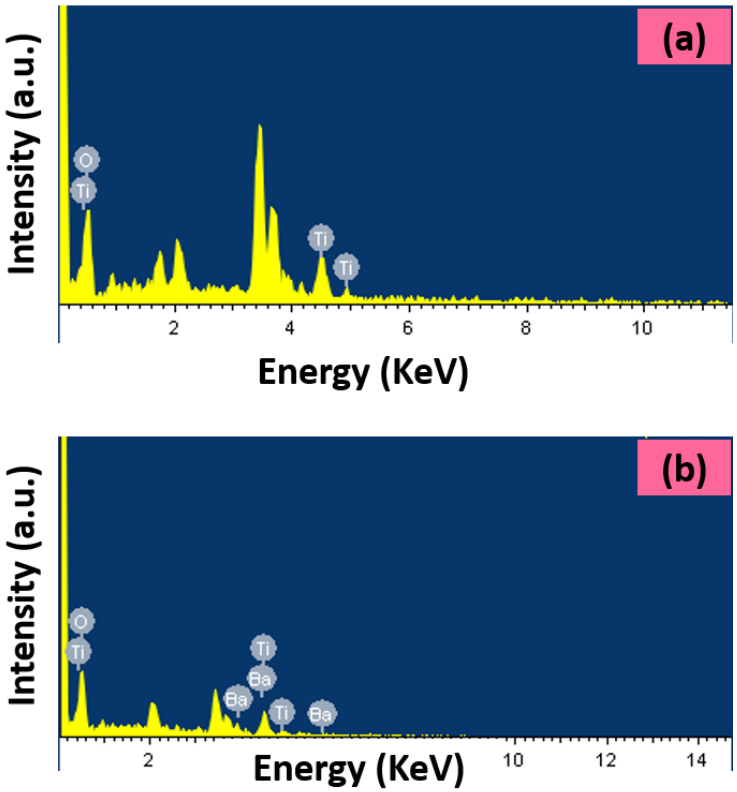

Figure S2. EDX spectra of (a) meso-TiO_2 and (b) meso-TiO_2-$Ba(OH)_2$ films.

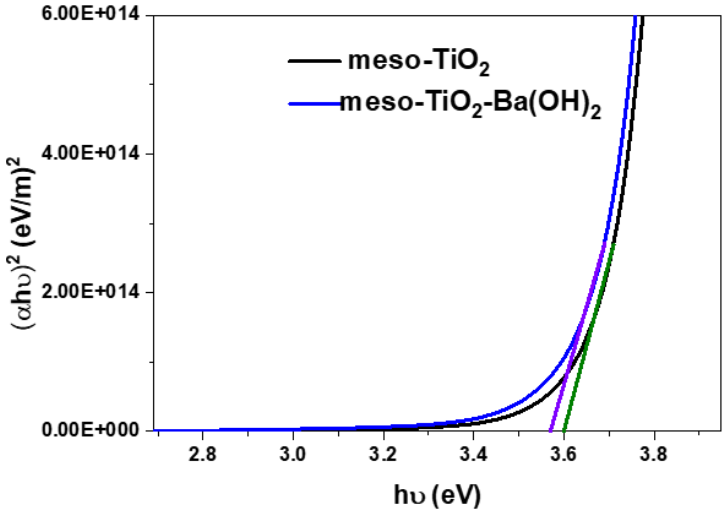

Figure S3. The plot of $(\alpha h\upsilon)^2$ versus $h\upsilon$ for meso-TiO_2 and meso-TiO_2-$Ba(OH)_2$ films.

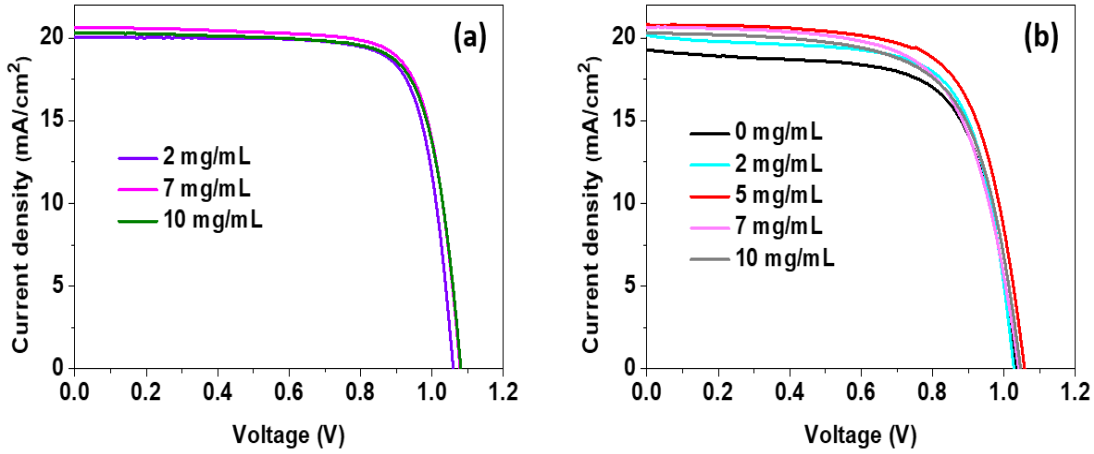

Figure S4. (a) J-V characteristics of the meso-TiO_2-$Ba(OH)_2$ ETL based perovskite solar cells under reverse scanning (RS). (b) J-V characteristics of the meso-TiO_2 and meso-TiO_2-$Ba(OH)_2$ ETL based perovskite solar cells under forward scanning (FS).

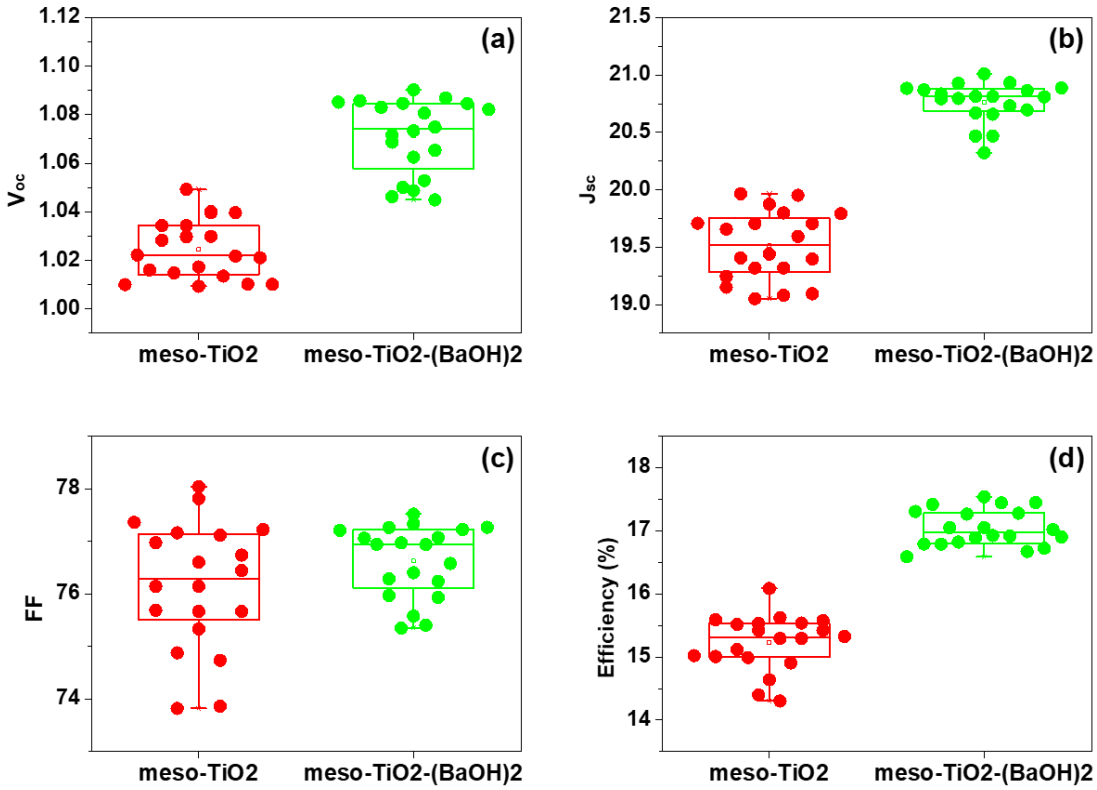

Figure S5. Statistical distribution of the perovskite solar cells with meso-TiO_2 and meso-TiO_2-$Ba(OH)_2$ ETLs: (a) distribution of V_{oc}, (b) distribution of J_{sc}, (c) distribution of FF, and (d) distribution of PCE. The concentration of $Ba(OH)_2$ solution for spin casting was 5 mg/mL

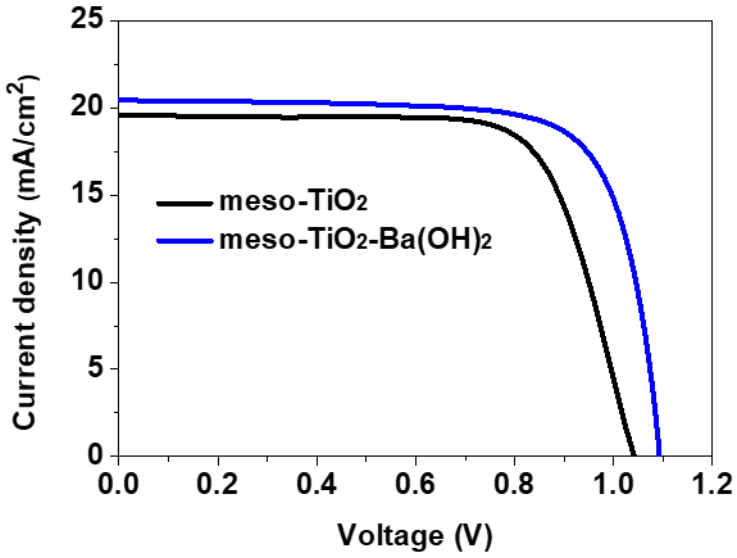

Figure S6**.** J-V characteristics of the meso-TiO_2 and meso-TiO_2-$Ba(OH)_2$ ETL based perovskite solar cells under reverse scanning direction after 25 days in ambient condition.

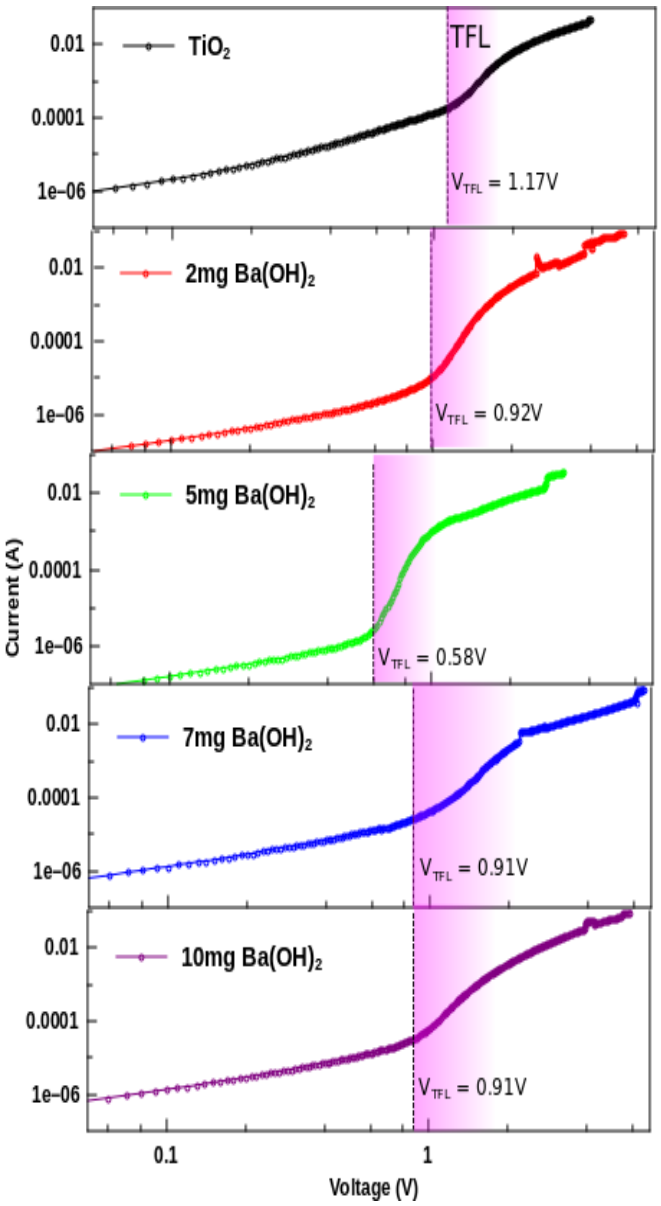

Figure S7. Current-voltage (I-V) characteristics for TiO_2 and TiO_2-$Ba(OH)_2$ films using space charge limited current (SCLC) model with device structure of FTO/TiO_2 or TiO_2-$Ba(OH)_2$/Au

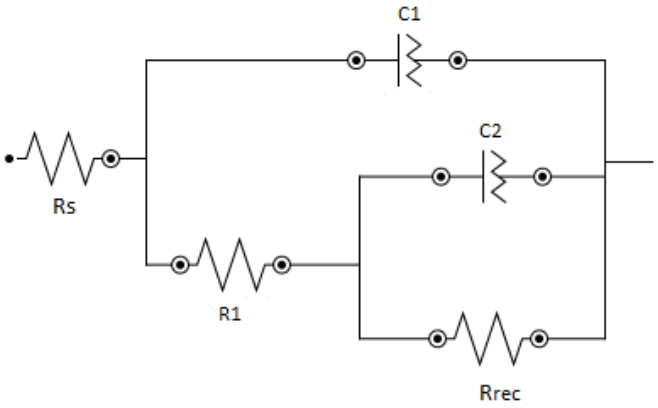

Figure S8. Equivalent circuit for the analysis of perovskite solar cells.

Table S1: The trap densities of TiO_2 and TiO_2-$Ba(OH)_2$ films with different $Ba(OH)_2$ concentrations.

$Ba(OH)_2$ modification	Trap filled limit voltage (V_{TFL})	**Trap Density** (N_t) **(cm^{-3})**
0 mg/mL	1.17	1.97×10^{18}
2 mg/mL	0.92	1.55×10^{18}
5 mg/mL	0.58	0.98×10^{18}
7 mg/mL	0.91	1.53×10^{18}
10 mg/mL	0.91	1.53×10^{18}

Table S2: The fitted parameters for EIS measurements acquired under dark condition.

$Ba(OH)_2$ modification	R_{series} (Ω)	R_{rec} (KΩ)
0 mg/mL	18.4	1.82
5 mg/mL	16.4	8.40
10 mg/mL	14.8	1.91